Environmental Science Nano

ROYAL SOCIETY OF CHEMISTRY

PAPER

View Article Online
View Journal | View Issue

Cite this: *Environ. Sci.: Nano*, 2026, **13**, 377

Iron-oxide nanoparticle release from jellyfish-based hydrogels for agricultural fertilization

Guy Avrahami,[a] Yinon Yecheskel,[a] Hadi Balous,[bc] Evyatar Ben Mordechay,[de] Shachar Richter[bc] and Ines Zucker *[a]

Iron (Fe) is an essential nutrient for plant growth, yet its bio-availability in soil is often restricted, limiting crop productivity. Conventional iron fertilizers, such as iron salts and chelates, suffer from inefficiencies and contribute to environmental concerns, including leaching and soil acidification. This study explores the use of jellyfish-based hydrogels as a slow-release carrier for iron-oxide nanoparticles (Fe-NPs) to enhance iron bio-availability in agricultural soils. Jellyfish-derived biomaterials offer a sustainable and biodegradable matrix with high water retention and tunable gel properties, making them an effective medium for controlled nutrient release. In this study, iron release was examined across various hydrogel formulations and environmental conditions to assess factors influencing nutrient bio-availability. The results demonstrate that iron release is highly dependent on hydrogel formulation, with key factors including hydrogel strength and the method of iron loading, such as nanoparticle selection and cross-linking with iron ions. Hydrogels cross-linked with iron ions released iron more rapidly than those cross-linked with calcium, while Fe_3O_4-containing hydrogels exhibited faster release than those incorporating $Fe(OH)_3$ nanoparticles. Additionally, monovalent ions accelerated hydrogel degradation through ion exchange, leading to increased iron release. Soil suspension experiments further confirmed that monovalent ions are a primary driver of hydrogel breakdown and iron release, whereas microbial activity has minimal impact on iron release. These findings highlight jellyfish-based hydrogels as an effective and biodegradable slow-release system, capable of modulating iron bio-availability based on environmental and soil conditions. This approach offers a promising, sustainable alternative to conventional iron fertilizers.

Received 25th May 2025,
Accepted 10th November 2025

DOI: 10.1039/d5en00505a

rsc.li/es-nano

Environmental significance

Iron deficiency in soils is a major challenge for global agriculture, often leading to decreased crop yields and reliance on conventional fertilizers, which contribute to nutrient runoff and environmental degradation. This study presents a novel approach for sustainable fertilization using jellyfish-based hydrogels as carriers for iron nanoparticles, enabling controlled and prolonged iron release. The methods herein not only repurpose an invasive species, but also minimize environmental pollution associated with traditional iron supplementation methods by leveraging biodegradable and marine-derived materials. The hydrogel's tunable properties allow for adaptation to various soil conditions, reducing waste and enhancing nutrient efficiency. This work advances environmentally responsible fertilization strategies, promoting soil health and resource sustainability in agriculture.

1. Introduction

The global population is continuously growing, with projections reaching 10 billion by 2050. To meet food demand, global agricultural production must increase by 70%.[1] However, the limited availability of land and the increase in food consumption have driven the adoption of intensive agricultural practices, which improve productivity but may also induce soil degradation.[2] Overuse of chemical fertilizers and excessive plowing can lead to depletion of essential nutrients and organic carbon, increased nutrient leaching, and changes in soil pH, all contributing to the harm of soil microbial communities essential for maintaining soil fertility and health.[3] Innovative, efficient, and sustainable solutions are needed to address these environmental challenges and ensure global food security.

[a] *School of Mechanical Engineering, Faculty of Engineering, Tel Aviv University, Tel Aviv 69978, Israel. E-mail: ineszucker@tauex.tau.ac.il; Tel: (+972) 73 3804581*
[b] *Department of Materials Science and Engineering, Faculty of Engineering, Tel Aviv University, Tel Aviv 69978, Israel*
[c] *University Center for Nano Science and Nanotechnology, Tel Aviv University, Tel Aviv, 6997801, Israel*
[d] *The Robert H. Smith Faculty of Agriculture, Food and Environment, The Hebrew University of Jerusalem, P.O. Box 12, Rehovot 7610001, Israel*
[e] *Agricultural Research Organization – Volcani Institute, Rishon LeZion 7505101, Israel*

Iron (Fe) is an essential micronutrient for processes like photosynthesis, respiration, and enzyme activity in plants. It plays a critical role in synthesizing chlorophyll and aiding in energy transfer, directly influencing crop productivity and quality.[4] Plants take up iron mainly through two strategies: most species reduce and absorb soluble Fe^{2+} at the rhizosphere, coupled with proton release, lowering the pH levels resulting in increased iron solubility (Strategy I), while gramineous plants release natural chelators, termed phytosiderophores (PS) that bind Fe^{3+} and the whole complex Fe^{III}–PS is taken up by a specialized transporter into the roots (strategy II). However, iron bio-availability in soils is often limited, particularly in alkaline or calcareous environments, leading to deficiencies that reduce yields and affect the nutritional value of food.[5] Furthermore, other scenarios may also drive low bioavailability of iron in the soil; for example, heavy chemical fertilizer application may change soil pH and thus affect iron solubility, or intensive cropping practices may increase nutrient demand.[6] Efficient iron delivery to plants can enhance crop yields and improve their nutritional value, and thereby affect human nutrient consumption.[7] Typical seasonal average Fe uptake in major crops ranges from approximately 1–5 mg Fe m^{-2} per day under a 100 day active growth period. These values—reported for maize,[8] wheat,[9] rice[10] and citrus[11] fertilization studies—provide agronomic benchmarks for estimating suitable daily Fe-release targets from slow-release fertilizer formulations.

Iron fertilizers such as iron salts and chelates (*e.g.*, EDTA, EDDHA) are commonly used to address iron deficiency in crops,[12] but have significant limitations to their effectiveness. Iron salts, though low in cost, can react in the soil environment to form iron species that are unavailable to plants.[13] Iron chelates—though more effective than iron salts—can lead to environmental concerns, such as nutrient leaching into groundwater and soil acidification.[14] Furthermore, the biodegradation of chelates, such as EDTA, is limited due to their stable molecular structure and strong resistance to enzymatic attack, and can only occur in specific conditions. Consequently, their presence in the environment can lead to increased solubility and mobilization of heavy metals, potentially contaminating water sources and plants.[15,16] These challenges require the development of alternative, efficient, sustainable, and affordable iron fertilizers.

The use of nanoparticles (NPs) for fertilization shows promising advantages that make them an attractive alternative to conventional fertilizers. Use of zinc NPs, for example, has been demonstrated to increase photosynthetic rate, leaf chlorophyll, and total dry mass of maize crops in cold conditions.[17] Nevertheless, as the phytostimulators were sprayed directly on the leaves, these results do not represent the NPs–soil–root continuum. Fe, Cu, Co and Zn oxide NPs were shown to assist soybean plants in adapting to drought stress following seed soaking in NPs solutions, as indicated by an increase in shoot length and biomass.[18] Yet, this study (again) did not evaluate the above-mentioned continuum. A recent paper has shed light on the applicability and reliability of these reported results,[19] increasing the need for quality in-depth research regarding the release and bioavailability of NPs in the soil system.

When introduced as NPs into the soil system, iron uptake can occur either after the particles slowly dissolve and release ions or through their direct contact and entry into root tissues through cracks and gaps in the root membrane, as evidenced by root uptake of nanoplastic, depending on their size and surface properties.[20–22] NPs in general can be absorbed into plants through foliar and root uptake, with their small size and high surface area to volume ratio facilitating their easy interaction, diffusion, and entry into plant tissue.[23] The complex NP uptake mechanism is still under investigation and is not well defined as that of conventional iron minerals, such as ferric oxides and hydroxides, which are known to first solubilized in the rhizosphere through root-induced acidification and reduction of Fe^{3+} to Fe^{2+}, or by chelation with PS, after which the soluble Fe^{2+} is absorbed into root cells *via* specific membrane transporters.[24]

However, despite this potential for efficient uptake, the effectiveness of NPs in agricultural applications largely depends on their delivery system. The application of bare NPs as fertilizers might be ineffective and unsustainable due to multiple challenges, including uneven distribution in soil, rapid leaching, and poor bioavailability, all of which limit NP accessibility to plants.[25,26] Additionally, plants have a restricted capacity for nutrient absorption, and excessive concentrations can not only contribute to environmental concerns but also pose potential toxicity risks, leading to adverse effects on plant health and growth.[27] Therefore, a delivery system that ensures controlled release and efficient nutrient delivery is critical for optimizing NP use. For example, polyvinyl alcohol and starch polymeric blends have been used to encapsulate copper and zinc NPs, enabling the NPs' slow and controlled release to improve nutrient delivery and enhance plant growth.[28] Similarly, soy protein-based bioplastics loaded with zinc oxide NPs were used as a controlled-release fertilizer, which enhanced nutrient uptake efficiency while minimizing leaching into the soil.[29] Silica NPs were used as carriers for nutrient delivery, improving nutrient uptake efficiency and allowing for plant growth with reduced fertilizer input.[30] These examples illustrate how an effective scaffold as a slow-release carrier system may help fully harness the benefits of NP-based fertilizers.

Jellyfish (JF), which is experiencing a worldwide surge in supply due to global changes such as ocean warming, eutrophication, overfishing of predators, and coastal pollution,[31] is recognized as a high-supply, sustainable, and cost-effective resource for agriculture. The JF biomass contains mainly water (95–98%), as well as (such as glycoproteins and collagen), and salts.[32–34] JF pose a significant ecological and economical liability, disrupting marine ecosystems, damaging fisheries and aquaculture, and clogging industrial cooling systems.[35] Utilizing JF as a

resource can help mitigate these challenges by transforming it into a valuable and sustainable solution. JF, as an organic fertilizer, can enhance soil health by improving moisture content and nutrient availability, which leads to improved plant growth.[36] JF-based hydrogels have been used previously in tissue engineering for regenerative scaffolds,[37] as biocompatible carriers for drug delivery,[38] and in biomedical research on hydrogels of tailored degradation and mechanical properties.[39]

JF-based hydrogels have also been studied as carriers for copper NPs, demonstrating for the first time their potential as an effective fertilizer.[40] In the formulation used, alginate—as well as the negatively charged groups of the jellyfish biomass—were crosslinked with divalent positively-charged cations (Ca^{2+} or Cu^{2+}) in the crosslinking solution, and the jellyfish acted also as a nutritional filler and host for copper oxide nanoparticles (*i.e.*, the active component). This latter study evaluated copper release under several hydrogel formulations and environmental conditions, while demonstrating the biodegradability and biocompatibility of the hydrogels compared to commercial fertilizers. However, the application of Fe-based nanomaterials should be investigated in a more comprehensive manner, particularly by exploring the impact of a broad range of formulations and environmental factors on iron release. Such findings could help optimize the hydrogel's agricultural application.

This study explores the use of a JF-based hydrogel as a carrier for iron-oxide NPs designed for slow-release fertilization. The use of JF in the hydrogel provides a source of organic matter that can enhance soil health, adding to the overall sustainability of the fertilizer, and also transform an environmental and economic risk into a sustainable resource. The release of iron from the hydrogel was studied in different hydrogel formulations and environmental conditions, emulating various agricultural scenarios. By exploring iron release across different parameters, this study shows the potential of JF-based hydrogels to serve as a versatile and eco-friendly iron fertilizer, adaptable to different soil types and environmental conditions and enabling a tailored solution for sustainable agriculture.

2. Methods

2.1. Preparation of jellyfish-based hydrogel beads with iron-oxide nanoparticles

Commercial iron-oxide NPs were embedded in a jellyfish (JF)-based matrix to generate hydrogel beads which are referenced generally as Fe@JF bead (see Fig. S1 in the SI). The hydrogels were prepared based on published formulation protocol.[40,41] Briefly, alginic acid sodium salt (8 g, Sigma-Aldrich, United Kingdom) was mixed with 3.8 g iron hydroxide NPs (10 nm $Fe(OH)_3$, US Research Nanomaterials, United States) and the resultant mixture was slowly added to 200 mL deionized water (DI, Milli-Q Direct, Merck Millipore, Germany) while mixing, resulting in a final suspension of 4% sodium alginate (SA) and 1.9% $Fe(OH)_3$ NP by mass. The mixture was stirred overnight until homogeneous. JF (*Rhopilema nomadica*) was harvested from a power plant along the Mediterranean seashore in Israel, ground, and frozen until used. 300 g of the JF was then defrosted and poured into the sodium alginate–iron hydroxide suspension and mixed until homogenous, ultimately reaching a 40 : 60 SA : JF ratio and total iron concentration of 0.4%. Finally, 50 μL drops of the suspension were dropped using a 3 mm diameter pipette into a 2% calcium chloride ($CaCl_2{\cdot}2H_2O$, Thermo Scientific Chemicals, United States) solution while continuously stirring. The hydrogel beads spontaneously formed through cross-linking between the calcium ions and alginate. The hydrogels were kept in the $CaCl_2$ solution for five minutes, followed by washing with DI water to remove excess NPs and ions from the bead surfaces. The generated hydrogel beads were kept in 4 °C until used and will be referred hereafter as $Fe(OH)_3$@JF hydrogel beads.

The Fe@JF beads were synthesized in various other formulations to evaluate changes in the physicochemical properties of the beads and the resulting iron release. First, the effect of using different forms of Fe NPs was evaluated. To do so, $Fe(OH)_3$ NPs were replaced with magnetic iron-oxide NPs (8 nm Fe_3O_4, US Research Nanomaterials, United States) to generate Fe_3O_4@JF hydrogel beads. The protocol for this latter form was the same as described above, but required the use of overhead stirring instead of magnetic stirring while cross-linking. Next, the effect of using different sizes of hydrogel forms were evaluated. To do so, differently-sized hydrogel beads were generated by adjusting the dropping tip diameter from 3 mm to 0.8 mm, which decreased the drop size from 50 μL to 11 μL, respectively, leading to smaller hydrogel sizes (small $Fe(OH)_3$@JF hydrogel beads). To evaluate the effect of the cross-linking ion, a mixture of 2% $CaCl_2$ and 2% iron(III) chloride ($FeCl_3$, Thermo Scientific Chemicals, United States) was used as an alternative cross-linking solution for the generation of hydrogel beads. This cross-linking solution was used in two different experiments: once without any NPs to prepare hydrogel beads containing only iron ions (Fe^{3+}@JF hydrogel beads), and once with NPs to prepare hydrogel beads containing both iron ions and NPs ($Fe(OH)_3$ + Fe^{3+}@JF hydrogel beads). To evaluate iron release from dry hydrogel beads, compared to wet hydrogel beads, $Fe(OH)_3$@JF were dried by frozen in liquid nitrogen immediately after preparation, followed by lyophilization (FDL-10N-50-TD-MM, mrc, Israel). Finally, the effect of SA content was evaluated by changing the ratio between SA and JF, using 30 : 70, 40 : 60, and 50 : 50 SA : JF ratios when synthesizing the $Fe(OH)_3$@JF hydrogel beads. The formulation of hydrogel beads without iron follows the same procedure outlined above, with the omission of introducing the iron nanoparticles.

2.2. Characterization of jellyfish-based hydrogel beads with iron-oxide nanoparticles

Bead diameter was measured by image processing using ImageJ software with a sample of 30 beads of identical formulation. Water content was measured by the mass difference of freshly prepared beads before and after 24 hours of air drying at room temperature. Total iron content was determined by submerging a known mass of freshly prepared beads in 20% hydrochloric acid (HCl, Sigma-Aldrich, United States) for >24 hours to ensure complete dissolution of $Fe(OH)_3$ NPs. The dissolved iron solutions were then analyzed using inductively coupled plasma mass spectroscopy (ICP-MS, 7800, Agilent, US) to quantify the total iron which was subsequently expressed relative to the mass of the hydrogels. Imaging and energy dispersive X-ray spectroscopy (EDX) measurement of the hydrogel's surface was conducted using an environmental scanning electron microscope (ESEM, Quanta 200 FEG). The preparation of the sample included slicing the hydrogels with a scalpel and air-drying them overnight, followed by coating with a chromium as an electron conducting layer. Imaging of the $Fe(OH)_3$ and Fe_3O_4 NPs was conducted using a transmission electron microscope (TEM, Talos F200i S/TEM, Thermo Fisher Scientific, US). The zeta potentials of the NPs before and after release were quantified using electrophoretic mobility measurements (Zetasizer Ultra, Malvern Panalytical, UK). Fourier-transform infrared spectroscopy (FTIR, Nicolet iZ10, Thermo Fisher Scientific, US) was performed on JF, sodium alginate, $Fe(OH)_3$ NPs, and $Fe(OH)_3$ NPs after release from the hydrogels.

2.3. Iron release experiments

Release experiments of iron from hydrogel beads were conducted in triplicate using a 50 mL plastic tubes by suspending ~2 g of beads in 40 mL of either tap water, buffer solution or soil suspension, as detailed below. The tubes were stirred on a tube roller at 70 rpm at room temperature for the duration of the experiment, typically 20–25 days. Samples were taken from the solution at different time intervals, then acidified and diluted for ICP-MS analysis. To distinguish between particulate and dissolved iron, additional samples were first centrifuged (18 000*g*, 10 minutes) to remove iron NPs. The supernatant, representing the dissolved ion content, was then analyzed for iron concentration by ICP-MS.

To investigate iron release in different chemical conditions, three types of solutions were employed: tap water (pH of 8.3, conductivity of 795 μS cm^{-1} at 25 °C), buffer solutions, and soil suspensions. The soil suspensions were prepared by mixing DI water and agriculture soil at a 1 : 1 mass ratio and stirring overnight. Soils were taken from Nir Oz, Ein Hashlosha, and Saad (Israel). The soil characteristics are shown in Table S1. The mixture was centrifuged at 18 000*g* for 10 minutes to settle large soil particles before filtering the solution through a 0.45 μm filter to remove any excess particles. To eliminate bacteria and fungi from the soil suspension, the soil was heated in an oven at 160 °C for two hours[42] before preparation of the soil suspension. To decrease the monovalent ion content in the soil suspension, the soil was submerged in 1 M $CaCl_2$ solution and stirred overnight before preparation of the soil suspension. To measure the effect of solution pH, the release of iron from the hydrogels were tested in phosphate buffer (NaH_2PO_4, Na_2HPO_4) solutions at solution pHs of 5.5, 6.5, and 7.5. To measure the effect of temperature on iron release, experiments were conducted in a temperature-controlled shaker incubator (70 rpm) at 10, 18, and 25 °C. The effect of mechanical stress on the release of iron from the hydrogel beads was tested by pre-sonicating the beads using a sonication bath (S30H, Elma, Germany) for 0, 10, 20 minutes prior to the release experiment. Release was also conducted in KCl solution at three concentrations (10, 50 and 100 mM) to evaluate the effect of ionic strength on the release of iron from the beads.

3. Results and discussion

3.1. Fe@JF-based hydrogel bead characteristics

The physical characteristics of the synthesized hydrogel beads are summarized in Table 1. In all hydrogel formulations (aside from the small bead formulation), the average bead diameter was 5.0 ± 0.1 mm. When changing the droplet volume from 50 μL to 11 μL, hydrogel diameter decreased to 3.3 ± 0.4 mm. The average water content by mass range from 93.1% to 95.7%, which is similar to previous publications.[40] The average mass per hydrogel bead was 40.6 ± 2.6 mg for 50 μL droplets, and 10.8 ± 1.2 mg for 11 μL droplets. Although $Fe(OH)_3$ and Fe_3O_4 were added in different amounts due to their distinct empirical formulas, iron has a negligible impact on the overall hydrogel mass, since the final iron content by mass in all formulations was below 1%. Formulations that had different ratios between SA and JF (as described in section 2.1) had similar characteristics as $Fe(OH)_3$ @JF beads.

Fig. 1 shows images of the different hydrogel formulations. The color of the hydrogel beads was greatly affected by the source of iron. Hydrogel beads without any iron NPs or ions (Fig. 1A) had a translucent color. $Fe(OH)_3$@JF (Fig. 1B), small $Fe(OH)_3$@JF (Fig. 1C), and $Fe(OH)_3$ + Fe^{3+}@JF beads had a dark brown color due to the $Fe(OH)_3$ NPs. Fe_3O_4@JF (Fig. 1D) beads had a dark lack color from the Fe_3O_4 NPs and Fe^{3+}@JF (Fig. 1E) beads had a light brown color from the $FeCl_3$ solution. Fig. 1F shows an SEM image of a $Fe(OH)_3$@JF bead, where in a higher magnification (Fig. S2) iron NP aggregates can be seen on the surface. The aggregation of the NPs can be attributed to the relatively high concentration of iron NPs in the formulation process, and the presence of Ca^{2+} ions in the cross-linking solution (which induce aggregation in iron-oxide NPs).[43] The zeta potential for these NPs was approximately −11 mV (Table S2), which creates weak electrostatic repulsion and may further contribute to the aggregation.

Table 1 Characteristics of iron-containing jellyfish-based hydrogel beads (Fe@JF) of different formulations. Bead diameters were measured using ImageJ software >30 beads. The mass per bead was measured for >10 beads. Iron content represents mass percentage from fresh (wet) hydrogel beads, for 3 beads in 3 replicates

Fe@JF bead type	Diameter (mm)	Water content (%)	Mass (mg)	Iron content (%)
$Fe(OH)_3$@JF beads	5.2 ± 0.5	94.3 ± 0.4	40.5 ± 0.7	0.42 ± 0.03
Fe_3O_4@JF beads	5.1 ± 0.5	94.1 ± 0.5	37.2 ± 2.7	0.46 ± 0.04
Small $Fe(OH)_3$@JF beads	3.3 ± 0.4	93.1 ± 0.3	10.8 ± 1.2	0.43 ± 0.03
$Fe(OH)_3$ + Fe^{3+}@JF beads	4.9 ± 0.5	94.9 ± 0.1	43.5 ± 1.9	0.58 ± 0.02
Fe^{3+}@JF beads	4.9 ± 0.4	95.7 ± 0.1	41.1 ± 0.8	0.21 ± 0.02

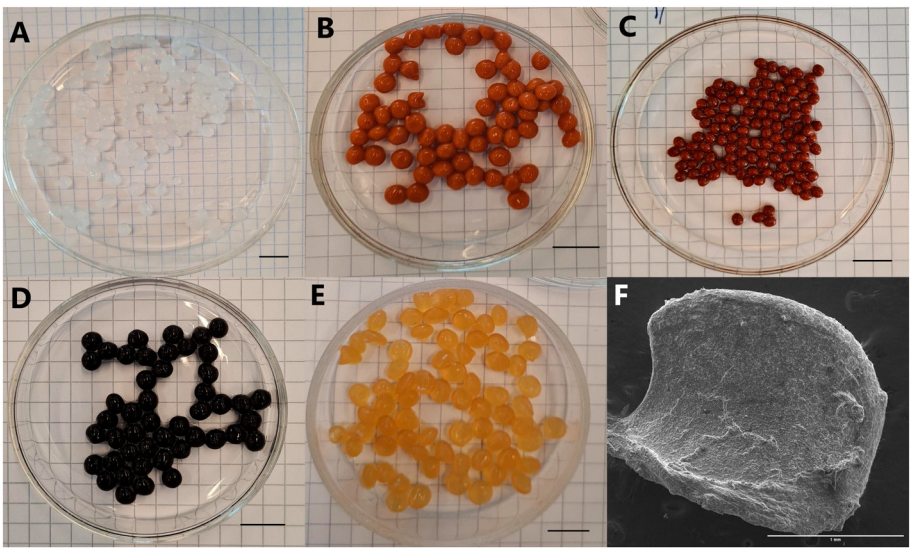

Fig. 1 Images of the iron-containing jellyfish-based hydrogel beads (Fe@JF). (A) Hydrogel beads formulated without iron NPs or ions. (B) Fe(OH)3@JF beads as well as (C) small $Fe(OH)_3$@JF beads, (D) Fe_3O_4@JF beads, (E) Fe^{3+}@JF beads and (F) environmental scanning electron micrograph (ESEM) of dried $Fe(OH)_3$@JF beads cross section. Scale bars represent 1 cm (black) and 1 mm (white). In images A–E, photos of the hydrogels were taken immediately after the formulation.

3.2. Iron release from jellyfish-based hydrogel beads

The release of iron from $Fe(OH)_3$@JF beads in the presence of tap water served as a benchmark in this study for comparison to iron release in other media. As shown in Fig. 2A, the total iron released reached approximately 0.9% of the total iron content after 21 days and then remained stable until day 30, making 20 days the chosen time frame for subsequent experiments. Separating the released Fe-NPs from dissolved ions after 21 days showed that iron was

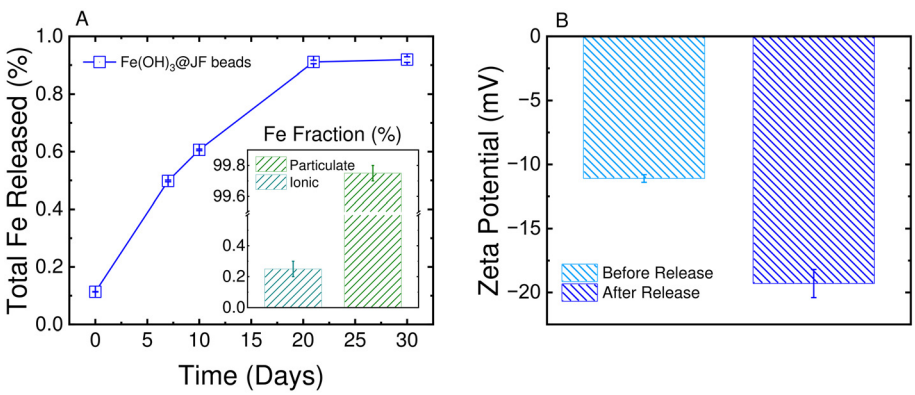

Fig. 2 (A) Percentage of iron release out of total iron content within $Fe(OH)_3$@JF beads in tap water after 30 days. Inset shows the fraction of ionic iron and particulate iron after 21 days. (B) Zeta potential of $Fe(OH)_3$ NPs before and after release from the $Fe(OH)_3$@JF beads.

primarily leached from the beads as particulate material, with dissolved ions accounting for only 0.25% of the iron released. The limited release of ions is expected due to the low dissolution rates of iron-(hydr)oxides minerals (including ferrihydrite, goethite, and hematite).[44] This limited release of iron ions suggests that upon release into the soil, iron oxide NPs will either be absorbed by the plant in particle form or undergo dissolution under varying soil conditions over time.

Previous studies on slow-release nano-fertilizers describe a swelling-controlled mechanism of polymeric nanocomposite in which water uptake expands the polymer network, loosens its structure and enables encapsulated nutrients or nanoparticles to diffuse out.[45] In our system, the beads were used as prepared and were already water-filled; accordingly, we observed only a minor increase in diameter (~2%), indicating negligible swelling under the tested conditions. Thus, any swelling-driven release within the timeframe of this experiment would be limited to particles located near the bead surface, consistent with the low iron release measured. In addition, size exclusion within the dense network likely contributes: small particles can more readily traverse the hydrogel matrix, whereas larger particles or aggregates are sterically retained. SEM imaging (Fig. S2) suggests that $Fe(OH)_3$ nanoparticles aggregated during bead preparation, which would further restrict their mobility and release.

Fig. 2B shows that after the release from the hydrogel matrix, the zeta potential of the NPs became more negative (−19 mV). The change in zeta potential after the release can be attributed to the coating of the NPs by the alginate, which has been shown to add negative surface charge to NPs.[46] The contribution of JF biomass to this change in zeta potential is less likely as JF has been shown to interfere with surface charge stabilization by reducing the absolute value of zeta potential of nanoplastics (100 nm).[47] Furthermore, FTIR measurements (Fig. S3) confirm interactions between alginate and iron nanoparticles after release, evidenced by the shift in the carboxylate peak (1597 cm^{-1} to 1635 cm^{-1}), splitting of the C–O–C peak (1027 cm^{-1} to 1037 and 1170 cm^{-1}), and splitting of the C–H peak (2915 cm^{-1} to 2835 and 2947 cm^{-1}).[48] The decrease in zeta potential of the nanoparticles (NPs) after release is a crucial aspect of this research. NPs with a more negative zeta potential experience greater electrostatic repulsion from negatively-charged soil particles.[49] This increased electrostatic repulsion enhances NP stability, reducing adsorption onto soil surfaces, promoting mobility through the soil matrix and consequently increase uptake potential by crops.

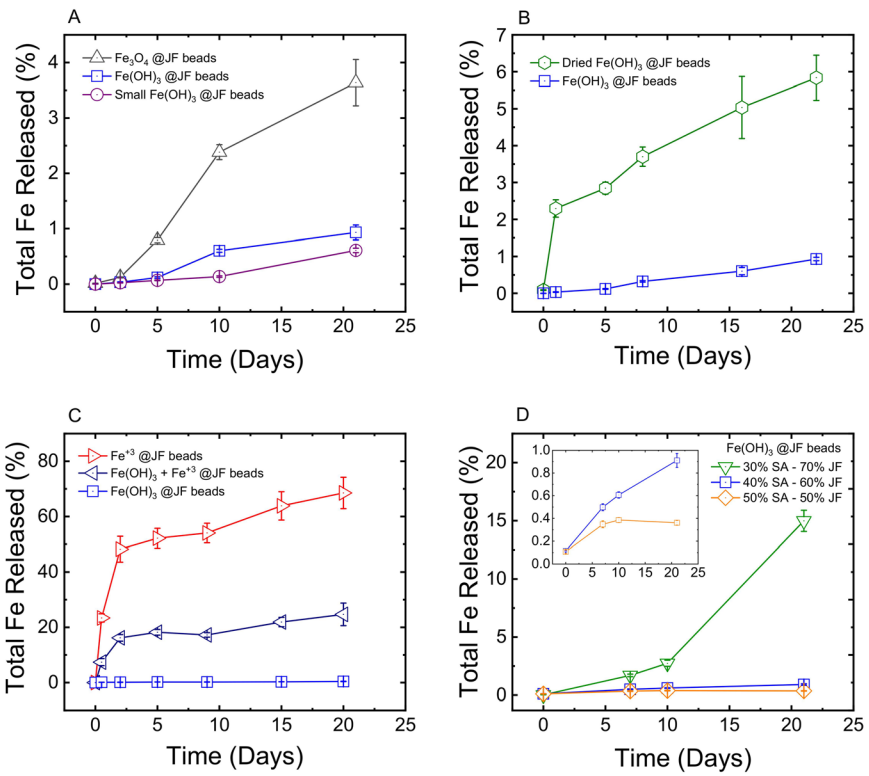

Fig. 3 Percentage of iron release out of total iron content for different hydrogel formulations, including iron release when using (A) different nanoparticles (NPs) and different hydrogel size, (B) freeze-dried hydrogels *vs.* fresh hydrogels, (C) hydrogel beads prepared in the presence of Fe^{3+} ions in the cross-linking solution (either with or without the addition of $Fe(OH)_3$ NP) compared with the benchmark formulation, $Fe(OH)_3$@JF, and (D) different ratios between sodium alginate and jellyfish (JF) during synthesis. The inset highlights the difference between 40% and 50% sodium alginate.

3.3. Changes in iron release based on hydrogel formulation

The release rate of iron from hydrogels incorporating different types of iron NPs was tested in tap water. Fig. 3A shows that Fe_3O_4 NPs reached more than 3.5% release of the total iron amount at day 20, while those with $Fe(OH)_3$ NPs showed a slower release rate of about 1% within the same time period. The higher release of Fe_3O_4 NPs indicates that they are weakly held within the hydrogel bead, leading to a faster release of iron from the hydrogel. The differences in iron release can be attributed to multiple factors related to the properties of the NPs. Fe_3O_4 NPs are smaller (8.5 ± 1.9 nm diameter) and more spherical, whereas $Fe(OH)_3$ NPs are larger (19.7 ± 5.1 nm diameter) and exhibit a more tubular shape, as seen in TEM imaging (Fig. S4). These differences likely influence how the NPs are encapsulated within the hydrogel matrix, contributing to variations in total iron release. Additionally, both NPs have zeta potentials with low absolute values (Table S2) and thus tend to aggregate, which may further impact their release behavior. Due to its chemical composition, each Fe_3O_4 NP contains approximately 2.1 times more iron than $Fe(OH)_3$. As a result, even if the same number of NPs are released, Fe_3O_4 hydrogels would release a greater total amount of iron, particularly when considering aggregation effects.

The effect of bead size on the release of iron NPs was examined using two different bead sizes, as detailed in Table 1 and shown in Fig. 3A. The release of iron from the small hydrogels was similar to that of the benchmark hydrogels in tap water, reaching ~0.6% release of total iron content after 20 days. The release of NPs is greatly affected by the size of the hydrogel pores which is affected by the hydrogel density.[50] The hydrogels' diameters and masses were used to calculate each hydrogel's density, and were found to be very similar to one another (density of the smaller hydrogels: 0.57 ± 0.05 mg mm^{-3}; density of the larger hydrogels: 0.55 ± 0.02 mg mm^{-3}). This similarity in density may explain why the release kinetics are similar for the two formulations.

The freeze-dried hydrogels exhibit a fast release after one day (2.3% of total iron content), followed by a continuous release that reaches approximately 5.5% of total iron content after 20 days (Fig. 3B). This difference in the amount of iron released from dried and wet hydrogels is attributed to the rehydration of the dried hydrogels, that leads to the faster release. Nucleation of ice during the freeze-drying process enhances the hydrogels porosity, and upon rehydration, the absorption of water may lead to increased pore size that allow NPs to escape from the hydrogel matrix.[51] Also, the swelling process can induce mechanical stress within the hydrogel, weakening its physical structure and causing the hydrogel to degrade faster.[52] Since the fresh hydrogels were already loaded with water, they remained more physically stable for the duration of the experiment as compared to the freeze-dried hydrogels, which endured both shrinking during freeze-drying and subsequent re-swelling in size during experimentation.

Hydrogels containing only ionic iron (Fe^{3+}@JF) showed a fast release in the first few days of the experiment, followed by a slower release that reached a release of about 70% of total iron content after 20 days, as shown in Fig. 3C. Similar kinetic trends were observed in the hydrogels containing both ionic iron and iron NPs ($Fe(OH)_3$ + Fe^{3+}@JF) however at a smaller final level of release, reaching about 20% iron release from the total iron content at 20 days. It is important to note that the observed differences in iron release are due to normalization relative to the total iron content in the hydrogel. When considering the absolute mass of iron released after 20 days, hydrogels containing both iron nanoparticles and iron ions released slightly more iron than those with only iron ions. However, the difference is minor because total amount of released iron (2.56 ± 0.02 mg for Fe^{3+}@JF beads and 2.73 ± 0.02 mg for $Fe(OH)_3$ + Fe^{3+}@JF beads) mainly originates from dissolved Fe^{3+} ions, while the contribution from the nanoparticles is negligible. Since the hydrogel beads were thoroughly washed before the experiment, the rapid release kinetics seen at the first days cannot be attributed to unbound iron ions, but more likely to ions that are close to the outer layer of the hydrogel, enabling an easier path for the ions into the solution. This is followed by a slower release of ions that diffused through a longer and possibly more complex pathway due to the hydrogel structure. The use of $FeCl_3$ in the cross-linking solution offers an alternative method for loading the hydrogels with iron but also offers another rate of iron release to the environment: a fast and immediate release of ions that is followed by a slower release of NPs as the hydrogel slowly degrades.

The effect of alginate content on iron release was studied by using three hydrogel formulations with different ratios between SA and JF. Hydrogels formulated with a 30 : 70 SA : JF ratio show the most rapid and significant release, reaching 15% release of the total iron after 20 days (Fig. 3D). The two other formulations (40 : 60 and 50 : 50 SA : JF) show similar release to one another, however, hydrogels formulated with 40 : 60 SA : JF had a slightly higher release than that of 50 : 50 SA : JF. The inverse relationship between SA relative content and iron release, *i.e.*, less SA augments iron release, may be attribute to the relationship between sodium alginate and the physical strength of the hydrogel. As the hydrogel formulation is based on the cross-linking between SA and Ca^{2+} ions, hydrogel beads with higher SA content result in a stronger structure and therefore show a slower release of iron NPs. Indeed calcium–alginate hydrogels (*i.e.*, 100% alginate) have been shown to form stable composites that restrict the release of embedded metal nanoparticles to negligible levels.[53–55] The 30 : 70 hydrogels degraded much faster due to a looser hydrogel matrix, which supports the release mechanism of NPs from the hydrogel, as described in the previous section.

Overall, the kinetic rates of iron release ranged from 0.14 ± 0.09 μg per day per bead to 8.05 ± 0.12 μg per day per bead,

demonstrating a wide tunability of release behavior among the different hydrogel formulations. Based on the typical Fe uptake rates of major crops described in the introduction, an estimated 100–650 beads per m^2 would be required to meet seasonal fertilization needs.

3.4. Changes in iron release based on environmental conditions

The release of iron from the hydrogel was studied in different environmental conditions as shown in Fig. 4. The hydrogel formulation used in this set of experiments was Fe@JF containing $Fe(OH)_3$ NPs and a SA : JF ratio of 40 : 60 (Table 1). The effect of solution pH was tested between 5.5 and 7.5, which are relevant for most agricultural crops.[56] As can be seen in Fig. 4A, hydrogels that were suspended in a buffer with pH of 5.5 released approximately 1.5% of total iron content, while those in pHs of 6.5 and 7.5 released 0.6% and 0.3%, respectively. The faster release of iron in the more acidic environment can be attributed to the faster degradation of the hydrogel matrix in lower pH, which can occur even at weakly-acidic conditions.[57]

The effect of temperature on the release of iron nanoparticles was examined (Fig. 4B), revealing that total iron release after 20 days decreases at lower temperatures. Hydrogels incubated at 25 °C released 0.8% of their total iron content, while those at 18 °C and 10 °C released 0.6% and 0.4%, respectively. This positive association between temperature and iron release can be attributed to the overall amount of system energy, which influences hydrogel behavior. Specifically, higher temperatures promote hydrogel swelling, leading to an expanded pore structure that facilitates greater nanoparticle diffusion.[58] However, since the tested temperatures are relatively low, the degree of swelling remains minimal, limiting the extent of iron release. The selected temperature range was based on the optimal soil conditions for most crops (12–30 °C), making the study of higher temperatures less relevant for agricultural applications.[59]

The hydrogels may encounter mechanical stress during their preparation, storage, or application. Studying the effects of sonication on the release behavior of iron can help predict and control how the hydrogels will perform under similar conditions. As can be seen in Fig. 4C, hydrogels that were subjected to mechanical stress through sonication had a much higher release after 20 days (up to 4%) than those that had not gone through the same process (<1%). The sonication process likely weakens the hydrogel matrix,[60] which reduces the cross-linking density and causes a faster release of iron. Understanding the effect of mechanical stress on the physical stability of the hydrogels can help in adapting them to different environmental conditions, for example, increasing cross-linking density in order to maintain stronger structure in harsh conditions.

The effect of monovalent ion concentration on the release of iron was studied by immersing the hydrogels in a KCl solution at three different concentrations. As can be seen in Fig. 4D, an increase in KCl concentration is correlated with an enhanced release of iron from the hydrogel matrix. Hydrogels suspended in 50 mM and 100 mM KCl released

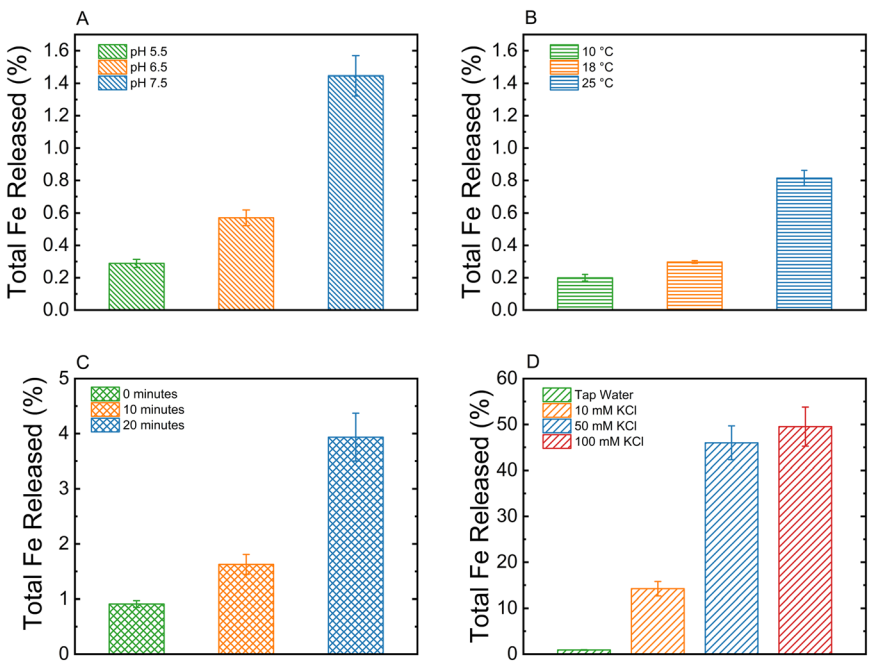

Fig. 4 Percentage of iron released after 20 days relative to the total iron content in $Fe(OH)_3$@JF beads across differing environmental conditions, including (A) effect of pH in phosphate buffer solution, (B) effect of temperatures, (C) effect of mechanical stress induced by varying bath sonication duration, and (D) effect of KCl concentration as a monovalent ion solution.

approximately 45% and 50% of their total iron content (respectively) after 20 days, whereas those in 10 mM KCl released 15% of their total iron content. This elevated release with higher KCl concentrations can be attributed to ion exchange processes occurring within the hydrogel matrix. Specifically, sodium alginate hydrogels, crosslinked with calcium ions, undergo partial cationic substitution once exposed to monovalent ions such as Na^+, K^+, and Li^+.[61] This exchange weakens the ionic crosslinking between Ca^{2+} and alginate, leading to a reduction in the structural integrity of the hydrogel.[62] Consequently, the hydrogel degrades at an accelerated rate, facilitating the more rapid release of iron. Understanding the impact of monovalent ions on hydrogel stability is crucial, as these ions are not only prevalent in soil environments,[63] but also serve as essential nutrients for crop growth, frequently introduced through fertilization.[64]

These release experiments provide a foundation for studying iron release in soil suspensions, where multiple environmental factors interact simultaneously. By first isolating these effects, a clearer understanding of how each condition influences hydrogel stability and iron availability was established. This knowledge allows the design of soil suspension experiments with a more informed approach, considering how these factors collectively impact release dynamics in real agricultural settings.

3.5. Changes in iron release in soil suspensions

The influence of different soil types on the release of iron nanoparticles was evaluated by immersing hydrogels in soil suspensions derived from three distinct soils (soil characteristics are shown in Table S1 and described in section 2.3). As shown in Fig. 5A, hydrogels immersed in soil suspensions prepared from Nir Oz (sandy soil, lower carbonate content, pH 7.5) and Saad soils (clay-loam soil, higher carbonate content, pH 7.6) released 21% and 12% of their total iron content, respectively, after 20 days. In contrast, hydrogels exposed to the soil suspension from Ein Hashlosha (loam soil, lower carbonate content, pH 7.5) released only 2% of the total available iron within the same timeframe. These values were higher than those observed under varying pH and temperature conditions but were comparable to the release observed in a 10 mM KCl solution, where 15% of the total iron content was released, as shown in section 3.4. This suggests that the increased iron release may be primarily driven by the presence of monovalent ions

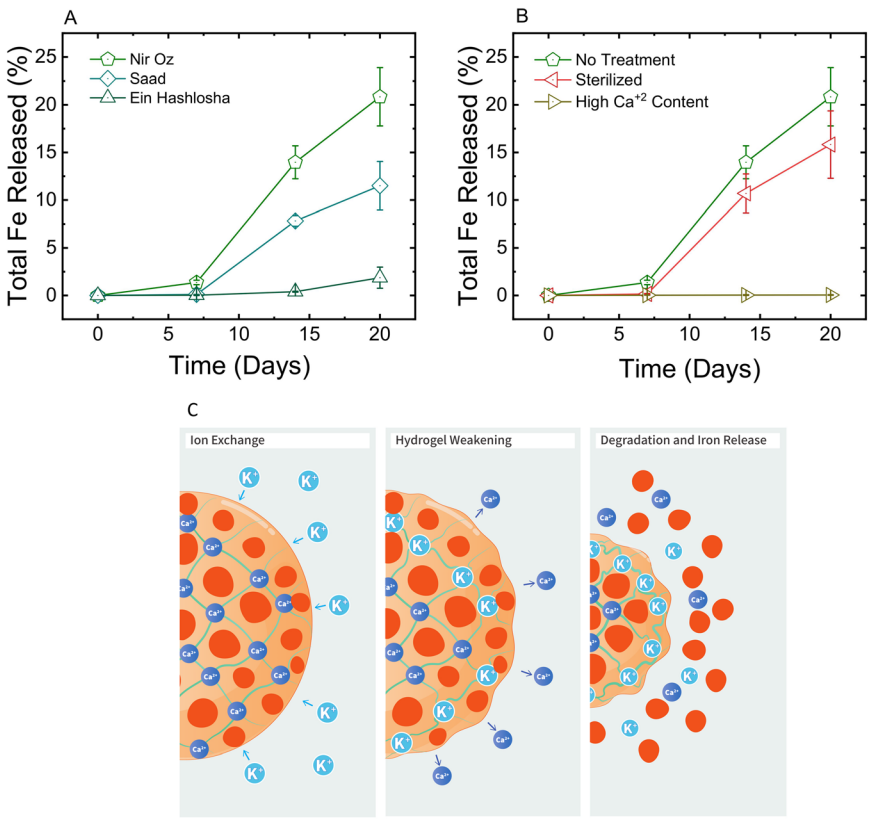

Fig. 5 Percentage of iron released after 20 days out of total iron content across different environmental conditions, including (A) soil suspensions prepared from Nir Oz, Saad, and Ein Hashlosha soils, (B) Nir Oz soil suspensions prepared without soil treatment, sterilized in 160 °C for two hours, and submerged in 1 M $CaCl_2$ to decrease the monovalent ion content. (C) Illustration of the release mechanism of iron in an environment with high monovalent ions concentration. Ion exchange occur between the K^+ and Ca^{2+} ions, the hydrogel matrix is weakened which facilitates degradation and iron release.

in the soil suspension, which contributes to the degradation of the hydrogel matrix,[62] thereby facilitating iron release. It should be noted that release to soil solution (or water) did not change the NP crystal structure (Fig. S5) which is important in the context of bioavailability of Fe following release.

To isolate the effects of monovalent ions and microbial activity on iron release, the experiment was repeated using microbial-activity-reduced soils (Nir Oz soil, treated to reduce microbial activity) and divalent-ions-dominant soils (Nir Oz soil, treated to reduce monovalent ion content). As shown in Fig. 5B, hydrogels immersed in a soil suspension where bacteria and fungi were inactivated exhibited a similar release pattern to those in untreated soil suspension, reaching 16% total iron release. In contrast, hydrogels immersed in soil suspension treated to reduce monovalent ion content showed minimal iron release, with only 0.1% of total iron released after 20 days, which was less than total iron released in tap water. Notably, hydrogel degradation was observed, as indicated by a visible reduction in their size over time (Fig. S6 and Table S3). Hydrogels immersed in untreated Nir Oz soil suspension and in a suspension treated to remove bacteria and fungi decreased in diameter by 16%, whereas those in soil suspension treated to reduce monovalent ion content exhibited no visible change in diameter. This suggests that the primary mechanism of iron release under these conditions is the gradual breakdown of the hydrogel matrix (illustrated in Fig. 5C), which facilitates nanoparticle release into the surrounding environment. This effect is primarily driven by ion exchange between Ca^{2+} ions in the hydrogel matrix and monovalent ions in the suspension, which weakens the hydrogel structure, accelerates degradation, and consequently promotes iron release.[62] The predominant cations identified in each soil sample were Ca^{2+}, K^{+}, Mg^{2+}, and Na^{+} (Table S4). These findings support the proposed release mechanism, as the Nir Oz soil suspension, which exhibited the highest iron release, contained high monovalent to divalent ions ratio with Na^{+} and K^{+} account for approximately 48% of the total ion content. In contrast, the proportion of monovalent ions in Saad and Ein Hashlosha soils was only 37% and 25%, respectively, which are correlated with their lower release rates. The observed differences in hydrogel degradation further support this mechanism, as structural weakening directly influences the extent of nanoparticle diffusion into the suspension.

4. Conclusion

This study demonstrated the potential of jellyfish-based hydrogels as a slow-release carrier for iron-oxide nanoparticles, offering a sustainable alternative to conventional iron fertilizers. The release of iron was found to be highly dependent on hydrogel formulation, where factors such as hydrogel strength, nanoparticle selection, and crosslinking with iron ions significantly influenced release behavior. Hydrogels crosslinked with iron ions released iron more rapidly than those crosslinked with calcium, while Fe_3O_4-loaded hydrogels exhibited faster release than those containing $Fe(OH)_3$ nanoparticles. Environmental conditions further impacted iron availability, with monovalent ions accelerating hydrogel degradation through ion exchange, leading to increased iron release. Soil suspension experiments confirmed that monovalent ions are a primary factor driving hydrogel breakdown and iron release, while microbial activity has a minimal influence.

These findings suggest that a controlled-release fertilizer could be developed by adjusting the hydrogel formulation and highlight the importance of tailoring the formulations to specific soil conditions to optimize nutrient delivery. Overall, jellyfish-based hydrogels present a biodegradable, adaptable, and eco-friendly solution for slow-release iron fertilization, contributing to more sustainable agricultural practices. Future research should focus on field-scale evaluations and plant uptake efficiency to further assess their long-term agronomic benefits and environmental impact.

Conflicts of interest

The authors declare no competing financial interests.

Data availability

The data supporting this article have been included as part of the supplementary information (SI). Supplementary information is available. See DOI: https://doi.org/10.1039/d5en00505a.

Acknowledgements

The authors would like to express their gratitude to Israel Innovation Authority for funding this research, as well as our collaborators in the project: Prof. Benny Chefetz, Prof. Moshe Shenker, Asher Altman, Hillel Magen, and Dr. Tamila Gulakhmedova. We also thank Dr. Alex Gordin from the Adama Center for his support with the ICP-MS instrument, Dr. George Levi for his assistance with TEM measurements, Roman Belykh for his help in analyzing FTIR measurements, Prof. Maxim Sokol (as well as Shira Gavriely and Bar Favelukis) for their help with XRD analysis, and Keren Faigon for her contributions to graphic design. SR acknowledges support from the Israeli Ministry of Environmental Protection.

References

1 M. van Dijk, T. Morley, M. L. Rau and Y. Saghai, *Nat Food*, 2021, **2**, 494–501.
2 H. I. Bedolla-Rivera, M. de la L. X. Negrete-Rodríguez, F. P. Gámez-Vázquez, D. Álvarez-Bernal and E. Conde-Barajas, *Agronomy*, 2023, **13**, 2166.
3 C. Vergara Cid, G. V. Ferreyroa, M. L. Pignata and J. H. Rodriguez, *J. Plant Nutr.*, 2020, **44**, 1131–1140.

4 S. A. Kim and M. Lou Guerinot, *FEBS Lett.*, 2007, **581**, 2273–2280.
5 S. Celletti, S. Astolfi, N. Guglielmo, G. Colla, S. Cesco and T. Mimmo, *Agronomy*, 2020, **10**, 1942.
6 Y. Zuo and F. Zhang, *Plant Soil*, 2010, **339**, 83–95.
7 M. Li, S. Watanabe, F. Gao and C. Dubos, *Plants*, 2023, **12**, 384.
8 P. Malathi and K. M. Sellamuthu, *Curr. J. Appl. Sci. Technol.*, 2022, **41**, 18–22.
9 B. Singh Chandel, D. Verma and A. Kumar Upadhaya, *Ann. Plant Soil Res.*, 2013, **15**, 39–42.
10 W. Butsai, W. Kaewpradit, D. L. Harrell and A. Polthanee, *Sustainability*, 2022, **14**, 15756.
11 M. R. Martínez-Cuenca, A. Quiñones, B. Martínez-Alcántara, J. Millos and F. Legaz, *Plants*, 2021, **10**, 79.
12 A. Arcas, S. López-Rayo, A. Gárate and J. J. Lucena, *Plants*, 2024, **13**, 819.
13 J. J. Lucena, in *Iron nutrition in plants and Rhizospheric microorganisms*, ed. L. L. Barton and J. Abadia, Springer, Netherlands, 1st edn, 2006, pp. 103–128, DOI: 10.1007/1-4020-4743-6_5.
14 L. H. Wu, Y. M. Luo, X. R. Xing and P. Christie, *Agric., Ecosyst. Environ.*, 2004, **102**, 307–318.
15 I. S. S. Pinto, I. F. F. Neto and H. M. V. M. Soares, *Environ. Sci. Pollut. Res.*, 2014, **21**, 11893–11906.
16 N. H. Almeaiweed, S. S. Aloud, K. D. Alotaibi, F. Alotaibi and B. Alshebel, *Sustainability*, 2025, **17**, 3745.
17 K. Ratajczak, H. Sulewska, K. Panasiewicz, A. Faligowska and G. Szymańska, *Agriculture*, 2023, **13**, 569.
18 T. M. Linh, N. C. Mai, P. T. Hoe, L. Q. Lien, N. K. Ban, L. T. T. Hien, N. H. Chau and N. T. Van, *J. Nanomater.*, 2020, **2020**, 4056563.
19 M. Frank and S. Husted, *Plant Soil*, 2024, **496**, 257–267.
20 P. Rai, S. Sharma, S. Tripathi, V. Prakash, K. Tiwari, S. Suri and S. Sharma, *Plant Nano Biol.*, 2022, **2**, 100017.
21 G. Liang, *Plant Commun.*, 2022, **3**, 100349.
22 Z. Yu, X. Xu, L. Guo, R. Jin and Y. Lu, *Sci. Total Environ.*, 2024, **907**, 168155.
23 X. Wang, H. Xie, P. Wang and H. Yin, *Materials*, 2023, **16**, 3097.
24 J. Morrissey and M. Lou Guerinot, *Chem. Rev.*, 2009, **109**, 4553–4567.
25 A. Munir, M. A. Salah, M. Ali, B. Ali, M. H. Saleem, K. G. B. A. Samarasinghe, S. I. S. De Silva, S. Ercisli, N. Iqbal and M. Anas, *BioNanoSci.*, 2024, **14**, 3846–3863.
26 K. K. Verma, X. P. Song, H. D. Degu, D. J. Guo, A. Joshi, H. R. Huang, L. Xu, M. Singh, D. L. Huang, V. D. Rajput and Y. R. Li, *Chem. Biol. Technol. Agric.*, 2023, **10**, 111.
27 P. Marschner, *Mineral Nutrition of Higher Plants*, Academic Press, 2012.
28 R. Kumar, M. Ashfaq and N. Verma, *J. Mater. Sci.*, 2018, **53**, 7150–7164.
29 M. Jiménez-Rosado, V. Perez-Puyana, P. Sánchez-Cid, A. Guerrero and A. Romero, *Polymers*, 2021, **13**, 486.
30 C. B. Adams, J. E. Erickson and L. Bunderson, *Agrosyst., Geosci. Environ.*, 2020, **3**, e20006.
31 S. H. Lee, L. C. Tseng, Y. Ho Yoon, E. Ramirez-Romero, J. S. Hwang and J. Carlos Molinero, *Environ. Int.*, 2023, **171**, 107699.
32 M. C. Gomez-Guillen, B. Gimenez, M. E. Lopez-Caballero and M. P. Montero, *Food Hydrocolloids*, 2011, **25**, 1813–1827.
33 M. Urai, T. Nakamura, J. Uzawa, T. Baba, K. Taniguchi, H. Seki and K. Ushida, *Carbohydr. Res.*, 2009, **344**, 2182–2187.
34 R. Pearson, R. Tellam, B. Xu, Z. Zhao, M. D. P. Willcox and K. Kongsuwan, *Bioscience Methods*, 2011, **2**, 21–30.
35 S. H. Lee, M. Scotti, S. Jung, J. S. Hwang and J. C. Molinero, *Hydrobiologia*, 2023, **850**, 2855–2870.
36 I. Emadodin, T. Reinsch, A. Rotter, M. Orlando-Bonaca, F. Taube and J. Javidpour, *Environ. Sustainability*, 2020, **3**, 105–115.
37 L. Riacci, A. Sorriento and L. Ricotti, *Gels*, 2021, **7**, 238.
38 Z. Ahmed, L. C. Powell, N. Matin, A. Mearns-Spragg, C. A. Thornton, I. M. Khan and L. W. Francis, *Mar. Drugs*, 2021, **19**, 405.
39 D. Salthouse, P. D. Goulding, S. L. Reay, E. L. Jackson, C. Xu, R. Ahmed, A. Mearns-Spragg, K. Novakovic, C. M. U. Hilkens and A. M. Ferreira, *Front. Bioeng. Biotechnol.*, 2024, **12**, 1391728.
40 S. Gavriely, T. Gulakhmedova, Y. Yecheskel, A. E. Rubin, B. Xing, S. Richter and I. Zucker, *NanoImpact*, 2022, **27**, 100417.
41 L. R. Steinberger, T. Gulakhmedova, Z. Barkay, M. Gozin and S. Richter, *Adv. Sustainable Syst.*, 2019, **3**, 1900016.
42 H. Li, L. Liu, C. Li, X. Liu, N. Ziadi and Y. Shi, *J. Soil Sci. Plant Nutr.*, 2023, **23**, 3979–3990.
43 L. Chekli, S. Phuntsho, M. Roy, E. Lombi, E. Donner and H. K. Shon, *Water Res.*, 2013, **47**, 4585–4599.
44 U. Schwertmann, *Plant Soil*, 1991, **130**, 1–25.
45 M. S. Haydar, D. Ghosh and S. Roy, *Plant Nano Biol.*, 2024, **7**, 100058.
46 M. K. Waqas, S. Safdar, M. Buabeid, A. Ashames, M. Akhtar and G. Murtaza, *J. Exp. Nanosci.*, 2022, **17**, 522–534.
47 E. A. Ben-David, M. Habibi, E. Haddad, M. Sammar, D. L. Angel, H. Dror, H. Lahovitski, A. M. Booth and I. Sabbah, *Sci. Total Environ.*, 2023, **869**, 161824.
48 H. Daemi and M. Barikani, *Sci. Iran.*, 2012, **19**, 2023–2028.
49 M. E. Sumner and W. P. Miller, in *Methods of Soil Analysis: Part 3, Chemical Methods*, ed. D. L. Sparks, A. L. Page, P. A. Helmke, R. H. Loeppert, P. N. Soltanpour, M. A. Tabatabai, C. T. Johnston and M. E. Sumner, Soil Science Society of America and American Society of Agronomy, Madison, WI, 1996, ch. 40, pp. 1201–1229.
50 J. Li and D. J. Mooney, *Nat. Rev. Mater.*, 2016, **1**, 16071.
51 K. Odziomek, A. K. Drabczyk, P. Kościelniak, P. Konieczny, M. Barczewski and K. Bialik-Wąs, *Pharmaceuticals*, 2024, **17**, 1512.
52 A. Leon-Cecilla, F. J. Vazquez-Perez and C. Gila-Vilchez, L. Álvarez de Cienfuegos and M. T. Lopez-Lopez, *Gels*, 2023, **9**, 39.

53 A. N. Bezbaruah, S. Krajangpan, B. J. Chisholm, E. Khan and J. J. Elorza Bermudez, *J. Hazard. Mater.*, 2009, **166**, 1339–1343.
54 C. J. Kearney, H. Skaat, S. M. Kennedy, J. Hu, M. Darnell, T. M. Raimondo and D. J. Mooney, *Adv. Healthcare Mater.*, 2015, **4**, 1634–1639.
55 S. Lilhare, S. B. Mathew, A. K. Singh and S. A. C. Carabineiro, *Nanomaterials*, 2021, **11**, 1345.
56 S. Oshunsanya, *Soil pH for Nutrient Availability and Crop Performance*, IntechOpen, London, 2019.
57 J. Zhang, C. Hurren, Z. Lu and D. Wang, *Int. J. Biol. Macromol.*, 2022, **222**, 1723–1733.
58 H. Malektaj, A. D. Drozdov and J. deClaville Christiansen, *Int. J. Mol. Sci.*, 2023, **24**, 5064.
59 P. K. Sharma and S. Kumar, *Soil Physical Environment and Plant Growth: Evaluation and Management*, Springer International Publishing, 2023.
60 R. Ebrahimi, H. G. Mohammadi, R. S. Ahmadabad and M. Rahmani, *Int. J. Energy Environ. Eng.*, 2010, **1**, 65–73.
61 J. C. Breger, B. Fisher, R. Samy, S. Pollack, N. S. Wang and I. Isayeva, *J. Biomed. Mater. Res., Part B*, 2015, **103**, 1120–1132.
62 C. Kaliampakou, N. Lagopati, E. A. Pavlatou and C. A. Charitidis, *Gels*, 2023, **9**, 857.
63 G. V. Subbarao, O. Ito, W. L. Berry and R. M. Wheeler, *Crit. Rev. Plant Sci.*, 2003, **22**, 391–416.
64 J. Sardans and J. Peñuelas, *Glob. Ecol. Biogeogr.*, 2015, **24**, 261–275.